Biosensors and Bioelectronics 249 (2024) 115988

Contents lists available at ScienceDirect

Biosensors and Bioelectronics

journal homepage: www.elsevier.com/locate/bios

Micromotor-based electrochemical immunoassays for reliable determination of amyloid-β (1–42) in Alzheimer's diagnosed clinical samples.

José M. Gordón Pidal [a], María Moreno-Guzmán [b], Ana Montero-Calle [c], Alejandro Valverde [d], José M. Pingarrón [d], Susana Campuzano [d,**], Miguel Calero [c], Rodrigo Barderas [c,***], Miguel Ángel López [a,e], Alberto Escarpa [a,e,*]

[a] Department of Analytical Chemistry, Physical Chemistry and Chemical Engineering, Faculty of Sciences, University of Alcalá, Ctra. Madrid-Barcelona, Km. 33.600, Alcalá de Henares, 28802, Madrid, Spain
[b] Department of Chemistry in Pharmaceutical Sciences, Analytical Chemistry, Faculty of Pharmacy, Complutense University of Madrid, Plaza Ramón y Cajal, s/n, 28040, Madrid, Spain
[c] Chronic Disease Programme, UFIEC, Carlos III Health Institute, Majadahonda, Madrid, 28220, Spain
[d] Department of Analytical Chemistry, Faculty of Chemistry Science, Complutense University of Madrid, Pza. de las Ciencias 2, Madrid, 28040, Spain
[e] Chemical Research Institute "Andrés M. Del Rio", University of Alcalá, Madrid, Spain

ARTICLE INFO

Keywords:
Screen printed electrodes
Brain tissue
Cerebrospinal fluid
Plasma
Alzheimer biomarkers
Dementia's disease

ABSTRACT

Alzheimer's disease (AD), in addition to being the most common cause of dementia, is very difficult to diagnose, with the 42-amino acid form of Aβ (Aβ-42) being one of the main biomarkers used for this purpose. Despite the enormous efforts made in recent years, the technologies available to determine Aβ-42 in human samples require sophisticated instrumentation, present high complexity, are sample and time-consuming, and are costly, highlighting the urgent need not only to develop new tools to overcome these limitations but to provide an early detection and treatment window for AD, which is a top-challenge. In recent years, micromotor (MM) technology has proven to add a new dimension to clinical biosensing, enabling ultrasensitive detections in short times and microscale environments.

To this end, here an electrochemical immunoassay based on polypyrrole (PPy)/nickel (Ni)/platinum nanoparticles (PtNPs) MM is proposed in a pioneering manner for the determination of Aβ-42 in left prefrontal cortex brain tissue, cerebrospinal fluid, and plasma samples from patients with AD. MM combines the high binding capacity of their immunorecognition external layer with self-propulsion through the catalytic generation of oxygen bubbles in the internal layer due to decomposition of hydrogen peroxide as fuel, allowing rapid biodetection (15 min) of Aβ-42 with excellent selectivity and sensitivity (LOD = 0.06 ng/mL). The application of this disruptive technology to the analysis of just 25 μL of the three types of clinical samples provides values concordant with the clinical values reported, thus confirming the potential of the MM approach to assist in the reliable, simple, fast, and affordable diagnosis of AD by determining Aβ-42.

1. Introduction

Alzheimer's disease (AD) is the most prevalent cause of dementia among the elderly (Alzheimer's disease facts and figures, 2021). It is a brain disorder that slowly and progressively impairs cognition, thinking skills, and the ability to independently carry out basic tasks. Statistics currently rank AD between the 3rd and 6th leading cause of death in the aged population. Data from AD International estimated that over 55 million people worldwide were living with dementia in 2020 and 60% of them have AD. These will almost double every 20 years, reaching 78

* Corresponding author: Department of Analytical Chemistry, Physical Chemistry and Chemical Engineering, University of Alcalá, Ctra. Madrid-Barcelona, Km. 33.600, Alcalá de Henares, 28802, Madrid, Spain.
** Corresponding author.
*** Corresponding author.
E-mail addresses: susanacr@quim.ucm.es (S. Campuzano), r.barderasm@isciii.es (R. Barderas), alberto.escarpa@uah.es (A. Escarpa).

https://doi.org/10.1016/j.bios.2023.115988
Received 21 November 2023; Received in revised form 22 December 2023; Accepted 27 December 2023
Available online 31 December 2023

million in 2030 and 139 million in 2050. The total societal burden of AD dementia was estimated at €232 billion in Europe in 2015, and $958 billion worldwide (Lane et al., 2018; Masters et al., 2015). Besides old age, there are other risk factors for AD development, such as environmental factors (Baumgart et al., 2015; Brown et al., 2005), lifestyle choices (Niccoli and Partridge, 2012), susceptibility genes, and other diseases (Franzmeier et al., 2019; Perry et al., 2016). Despite efforts and current advances to improve the diagnosis and management of AD (Hampel et al., 2020; Nguyen et al., 2021; Se Thoe et al., 2021), which results in a late application of the therapeutic actions, this disease is currently incurable (Calabrò et al., 2021). This implies an increase in mortality and higher societal costs, being needed for the development of new prevention modalities (Wesenhagen et al., 2020).

The definitive diagnosis of AD still requires post-mortem verification, as current technologies are not specific enough about the disease, become late in its development, or are very invasive (Jack et al., 2010; Montero-Calle et al., 2020; San Segundo-Acosta et al., 2019; Thorsell et al., 2010). Additionally, most AD patients are currently clinically diagnosed when symptoms appear and treatments are less effective (Palareti et al., 2016). Current AD diagnosis includes cerebrospinal fluid (CSF) and imaging biomarkers classified as: i) biomarkers of amyloid-β (Aβ) plaques, including cortical Aβ PET ligand binding and a high Aβ-42 or Aβ-42/Aβ-40 ratio in CSF; ii) biomarkers of fibrillary Tau, including high levels of phosphorylated Tau in CSF and cortical Tau PET ligand binding; and iii) biomarkers of neuronal damage, like high levels of total Tau in CSF, reduced FDG-PET metabolism, and brain atrophy on magnetic resonance imaging (Montero-Calle et al., 2023a; San Segundo-Acosta et al., 2019, 2021). Their analysis requires expensive and high-invasive techniques only available in specialized clinical settings. These examinations are important to identify non-AD pathological processes that can lead to cognitive decline and to search for biomarkers providing supportive features for the diagnosis of AD years before the appearance of symptoms. Although the incomplete verification of diagnostic biomarkers, strategies for their identification and quantification is a challenging area to apply effective therapies that imply a reduction of the disease progression and, therefore, brain deterioration as an alternative to classical methods (Lukiw et al., 2020; Montero-Calle et al., 2023a; Nguyen et al., 2021; San Segundo-Acosta et al., 2019, 2021; Se Thoe et al., 2021).

The main histological hallmarks of AD are extracellular deposits of amyloid plaques, caused by the accumulation of insoluble forms of Aβ peptide, and intracellular accumulations of neurofibrillary tangles (NFTs) formed by aggregates of hyperphosphorylated Tau (Deture and Dickson, 2019; Hampel et al., 2021; Murphy and Levine, 2010; Ono et al., 2016). The 42-amino-acid form of Aβ is the major constituent of the amyloid plaques (Selkoe and Schenk, 2003; Veloso et al., 2014). Aβ-42 is generated by the amyloidogenic proteolysis of the amyloid precursor protein (APP) via β- and γ-secretase (Selkoe, 2001). Aβ monomers tend to polymerize into soluble filaments to form oligomers of higher order and insoluble fibrils that accumulate forming the amyloid plaques and also in the walls of cerebral blood vessels (Shankar et al., 2008; Taylor et al., 2002). Therefore, the development of simple and sensitive methods to detect Aβ peptides to provide an early detection and treatment window for AD is a clear challenge.

In the last years, significant efforts have been made to measure the variation of Aβ-42 in human samples as a diagnostic biomarker of AD through fluorescence intensity distribution analysis (sFIDA) (Kühbach et al., 2016; Kulawik et al., 2018), fluorescence (Liu et al., 2018; Lv et al., 2016; Teoh et al., 2015; Xia et al., 2016), enzyme-linked immunosorbent assay (ELISA) (Ah et al., 2015; Klaver et al., 2010; Zhao et al., 2021), surface plasmon resonance (SPR) (Haes et al., 2005; Yi et al., 2015), colorimetric detection (Deng et al., 2018; Zhu et al., 2018), or electrochemical techniques (Qin et al., 2018; You et al., 2020; Zhou et al., 2021), among others. Yet, these methods require sophisticated instrumentation, present high complexity, are sample and time-consuming, and costly. Also, Alzheimer's patient samples are hard to obtain, so the development of novel diagnosis tools with low sample requirements is also needed. Therefore, due to the existing challenge of providing early detection and treatment for AD, there is a need to improve the simplicity, selectivity, and sensitivity of low-sample-based diagnostic methods to make AD diagnosis more affordable.

Micromotor (MM) technology has become a useful alternative and adds a new dimension to biosensing research (Feng et al., 2021; Gao et al., 2012; Veloso et al., 2014; Wang, 2016; Yuan et al., 2021). MM are microdevices that transform the energy from an external stimulus or a chemical reaction into kinetic energy through their autonomous movement along a solution (Wang, 2014). Particular attention has been given to tubular catalytic micromotors that can reach ultrafast speeds to perform complex analytical tasks. Among other protocols, these micromotors can be prepared by templated-based electrodeposition of polymers (Gao et al., 2012), metals (Zhao and Pumera, 2013), and carbon nanomaterials (Maria-Hormigos et al., 2016b), and can be smartly functionalized with a plethora of receptors, such as the most commonly used antibodies (Maria-Hormigos et al., 2016a; Pacheco et al., 2019; Yuan et al., 2020a, 2020b), enzymes (María-Hormigos et al., 2022), and aptamers (Gordón et al., 2022; Gordón Pidal et al., 2023). The chemical power of MM is based on catalytic decomposition (in the inner layer, mostly on Pt) of a fuel solution (commonly hydrogen peroxide) that entails a continuous movement of MM along the sample through bubble-propelled locomotion, enhancing the interactions of MM surface with the target analytes (Novotný et al., 2019) or improving the recognition event through specific biomolecular interactions (Pacheco et al., 2019), as well as the kinetics in relevant biological fluids and salt-rich environments. The bubble propulsion mechanism is based on two simultaneous events. On the one hand, the growth of the bubbles collapse onto the surface, and the impulse generated by the bubbles detached from the surface of MM, which results in a continued release of bubbles that impulse the micromotor in the opposite direction. The speed of MM is influenced by the radius and the frequency of the bubbles generated, which are dependent on the concentration of the fuel. Another point to take into account is the fluid mixing produced by the movement of MM (Mundaca-Uribe et al., 2021), which involves an acceleration of chemical processes, allowing ultrasensitive detections in short times in microscale environments, which avoid sample preparation if they are smartly functionalized (Maria-Hormigos et al., 2016a; Pacheco et al., 2019; Yuan et al., 2020b).

MM-based immunoassays (Molinero-Fernandez et al., 2020; Molinero-Fernández et al., 2020) and aptassays (Gordón et al., 2022, Gordón Pidal et al., 2023) have been demonstrated to be useful tools for diagnosis when sample availability is limited, such as in the case of neonatal sepsis. Due to these excellent results, here we are exploring the MM potency in the diagnosis of AD.

To this end, we propose for the first time an immunoassay approach based on the use of magneto-catalytic MM for the electrochemical determination of Aβ-42. The detection has been designed through an on-the-move approach using MM based on polypyrrole (PPy) due to its large functional groups to assess an efficient antibody functionalization and the PtNPs-based inner catalytic layer, which allow autonomous propulsion. This pioneering approach has been applied for the analysis of AD samples from the left prefrontal cortex brain tissue (BT), cerebrospinal fluid (CSF), and plasma samples.

2. Experimental

2.1. Reagents and solutions

Biotin (azide-free) anti-β-Amyloid (1–42) (c-$Ab_{Aβ-42}$) obtained from Biolegend was prepared in a phosphate-buffered saline (PBS solution pH 7.5 (2.7 mM KCl (99%), 0.1 M Na_2HPO_4 (99%) from Sigma-Aldrich; 138 mM NaCl (99%), 0.1 M NaH_2PO_4 from Panreac)). Human β-Amyloid Peptide (1–42) (Aβ-42) and HRP anti-β-Amyloid (1–16) (d-$Ab_{Aβ-42}$) antibody were obtained from Biolegend. Their corresponding dilutions

were prepared in 5% bovine serum albumin (BSA), purchased from Sigma Aldrich, in PBS pH 7.5 (PBS-BSA 5%) solution.

Streptavidin, N-hydroxysulfosuccinimide (NHSS), 1-ethyl-3-(3-dimethylaminopropyl) carbodiimide (EDC), and hydroquinone were purchased from Sigma-Aldrich (Madrid, Spain). Streptavidin, NHSS, and EDC were prepared in 2-(N-Morpholino) ethane sulfonic acid (MES) solution 0.1 M pH 5, obtained from Sigma-Aldrich. Hydrogen peroxide (H_2O_2) (30%) was purchased from Fisher Chemical. Hydroquinone and H_2O_2 solutions were prepared in phosphate buffer 0.1 M, pH 7 (PB).

Pyrrole-3-carboxylic acid, Potassium nitrate (99%), hexachloroplatinic (IV) acid (H_2PtCl_6), Nickel (II) sulfamate tetrahydrate ($H_4N_2NiO_6S_2$), Nickel (II) chloride hexahydrate ($Cl_2Ni–6H_2O$), dichloromethane, isopropanol, and ethanol were purchased from Sigma-Aldrich. Boric acid (H_3BO_3) (99.5%) was purchased from Fluka. 5 μm diameter conical pores polycarbonate membranes (PC) were purchased from Whatman. MicroPolish Alumina (0.05 μm) was purchased from Buehler.

All chemicals used were analytical-grade reagents. Deionized water was obtained from a Millipore Milli-Q purification system (18.2 MΩ cm at 25 °C).

Screen printed electrodes (SPCE) DRPC110 (3.4 × 1.0 × 0.05 cm (Length x Width x Height) and 4 mm Ø) were used.

2.2. Samples

BT, CSF, and plasma from the left prefrontal cortex from healthy controls and AD patient's postmortem verified with the disease were provided by the CIEN Foundation's Tissue Bank (BT-CIEN) with the written informed consent from all participants and complied with the ethical issues and brain bank's guidelines. These samples were stored at −20 °C until use. Protein extracts from the BT samples were obtained as previously described (Garranzo-Asensio et al., 2018; Montero-Calle et al., 2023a) and their concentration was measured by the Tryptophan method.

In total, 3 BT samples from healthy individuals (n = 1), and from AD patients at Braak IV (n = 1) and VI (n = 1) were analyzed. From plasma, a total of 3 samples from healthy individuals (n = 1), and from AD patients at Braak IV (n = 1) and V (n = 1) were used, together with 4 CSF samples from healthy individuals (n = 1), and AD patients at Braak IV (n = 1), V (n = 1), and VI (n = 1). The same BT, CSF, and plasma were measured with the MM and the SMCxPRO technologies.

The Institutional Ethical Review Board of the Spanish Research Center for Neurological Diseases Foundation (CIEN), the Instituto de Salud Carlos III, and the University of Alcalá de Henares approved this study on the analysis of biomarkers of Alzheimer's disease (CEID2021/4/108).

2.3. Apparatus

An electrochemical station μ-Autolab Type III (Eco Chemie, Utrecht, Holland) was used for template-assisted electrochemical deposition of PPy/Ni/PtNPs and to carry out the amperometric measurements. Advanced VortexMixer-ZX3 from VWR and Thermosaker TS-100 C from Biosan were used for incubation stages. For the handling of magnetic PPy/Ni/PtNPs, a Magnetic block DynaMag-2 obtained from ThermoFisher was used. Scanning electron microscopy (SEM) images were obtained with a JEOL JSM 6335 F instrument and X-ray analysis was performed through an EDX detector attached to a SEM instrument.

2.4. Electrochemical synthesis of tubular catalytic PPy/Ni/PtNPs MM

The conical pores of a PC membrane were treated with a sputtered thin gold film to perform it as a working electrode. The membrane was assembled onto a Teflon-plated cell covered with aluminum foil serving as an electrical contact to the working electrode for the subsequent electrodeposition. First, the outer layer was electropolymerized applying a voltage of 0.8 V until the current was stabilized from a solution containing 25 mM pyrrole-3-carboxylic acid and 7.5 mM KNO_3. An intermediate Ni layer is plated inside the PPY by galvanostatic method in two steps: initially, 10 pulses of 20 mA for 0.1 s for the generation of nucleation spots was carried out and continued by a constant current of −6 mA for 300 s to grow the Ni layer for a solution of 1.2 M $H_4N_2NiO_6S_2$, 82 mM $Cl_2Ni–6H_2O$ and 464 mM acid boric. Finally, the Pt layer was deposited by amperometry at −0.4 V for 750 s from an aqueous solution containing 4 mM of H_2PtCl_6 and 0.5 M boric acid. After the electrodeposition, the sputtered gold layer was gently hand-polished with 0.05 μm alumina slurry. The cleaned membrane was dissolved in CH_2Cl_2 for the release of MM (3 times, 15 min). Successive washing of the MM with isopropanol (3 times, 10 min), ethanol (2 times, 5 min), and water (1 time, 5 min) to get a neutral medium. All this process was performed using a magnet-holding block. All MM were stored in ultrapure water at 4 °C when not in use. The template preparation method resulted in reproducible MM with a similar shape and size. Next, with the use of an optical microscope, the number of micromotors is counted in 1 drop of 1 μL (n = 10) of the synthesized and washed batch, to know the concentration of micromotors/μL per synthesized batch.

2.5. Micromotor functionalization

The fabricated set of MM was functionalized in their outer layer with streptavidin to immobilize the c-$Ab_{Aβ-42}$. In this sense, a solution of MM was incubated with a 100 mM EDC/NHSS solution (50 μL for each 200 μL of MM) prepared in 0.1 M MES buffer, pH 5, for 30 min at 25 °C, to activate the carboxyl-terminated groups of the micromotor's surface. Then, the activated MM were washed 2 times with MES buffer, followed by the addition of streptavidin 400 μg/mL in 0.1 M MES buffer, pH 5.0, for 1 h at room temperature. Immediately, the MM were washed twice with 100 μL of MES buffer, and once with 100 μL of 0.1 M PBS buffer. Finally, the streptavidin-modified micromotors were incubated in a solution containing 25 μg/mL c-$Ab_{Aβ-42}$ for 30 min at room temperature. After that, the supernatants were removed and washed twice with 100 μL of PBS buffer, and then the MM were resuspended in 25 μL of PBS and maintained at 4 °C.

2.6. Aβ-MM immunoassay strategy

The proposed strategy is based on a sandwich-type immunoassay where anti-β-amyloid modified MM (5000 micromotors) were added to a solution (25 μL of total volume) containing the sample analyte (23 μL), d-$Ab_{Aβ-42}$ dissolved in PBS with BSA 5%, and H_2O_2 (2% final concentration) as MM fuel. The self-propulsion of MM, thanks to the catalytic reaction between the inner Pt layer and H_2O_2, provides for 15 min the on-the-fly biorecognition of the β-amyloid protein in the sample. Afterwards, the addition of 100 μL of PBS causes the MM to stop and, immediately, the supernatant was removed retaining the MM thanks to their intermediate magnetic layer and the aid of a magnet, followed by several washing steps with PBS.

2.7. Electrochemical measurements

The previously obtained MM-immunocomplexes were resuspended in 45 μL of hydroquinone (HQ) solution (1 mM) and transferred onto the surface of a commercial SPCE, where are retained by a small magnet located on the back of the working electrode surface to perform amperometric measurements at −0.2 V. Once the baseline was stabilized, 5 μL of H_2O_2 solution was added (5 mM final concentration) and the produced signal was recorded. The measurements were based on the difference between the steady-state and the background currents after the 200 s. These results were fitted to a four-parameter logistic equation using the software SigmaPlot 15.0 (Eq (1)).

$$i = \left(\frac{i_{max} - i_{min}}{1 + \left(\frac{EC_{50}}{x} \right)^{h}} + i_{min} \right)$$

i is the electrochemical signal, while i_{max} and i_{min} are the maximum and minimum current values of the calibration graph, respectively. EC_{50} is the value of the analyte concentration corresponding to 50% of i_{max}, and h is the hill slope.

The limit of detection (LOD) was calculated using the criteria 3 s/m and the limit of quantification (LOQ) 10 s/m. S was estimated as the standard deviation measuring the lowest protein concentration used in the calibration (0.2 ng/mL, n = 10), whereas m is the slope of the regression lineal obtained from the linear calibration plots.

2.8. SMCxPRO immunoassays

The high-sensitivity SMCxPRO instrument (Merck) was used for the measurement of total Aβ-42 (03-0146-00) in BT, CSF, and plasma samples following manufacturers' instructions. For the determination of Aβ-42 levels, plasma and CSF samples were 1/5 diluted, whereas 100 μg of each BT sample was analyzed.

2.9. Statistical analyses

p-values <0.05 were considered statistically significant. ROC (Receiver Operating Characteristic) curves and correlation between MM and SMCx data were obtained with R (version 3.6.2), using the "ModelGood" and the "Epi" packages to determine the diagnostic ability of the test (Montero-Calle et al., 2023b; Torrente-Rodríguez et al., 2022).

3. Results and discussion

3.1. MM-based immunoassay approach: strategy, characterization, and optimization

We hypothesize that the anti-Aβ-42 functionalized MM can perform the Aβ-42 determination towards a sandwich-type immunoassay efficiently using low clinical sample volumes. To this end, tubular MM was electro-synthetized by concentric layers with designed functions: PPy–COOH–streptavidin outer layer as immobilization support for capture anti-β-amyloid antibody, and internal PtNPs catalytic layer for the generation and ejection of oxygen bubbles from H_2O_2 used as fuel for driven catalytic propulsion. Also, a Ni intermediate layer for magnetic detection handling on the SPCE was electro-synthetized. A scheme of the sandwich-type MM-based immunoassay approach is shown in Fig. 1 (Top).

PPy/Ni/PtNPs MM characterization was carried out. SEM images revealed a well-defined conical shape (5 μm of width, 10 μm of height) of the MM (Fig. 1A). The synthesis efficiency towards the homogeneous distribution of the layer-by-layer MM electrosynthesis was demonstrated by the EDX analysis shown in Fig. 1B. They revealed its composition confirming the presence of C and N from PPy as the sensing layer, Ni as the magnetic layer, and Pt as the catalytic layer.

The on-the-fly immunoassay optimization procedures involve the study of those variables related to immunoassays together with those specific from the propulsion of MM into the sample solution and their interaction with the analyte.

Fig. S1A shows the influence of the number of MM on immunoassay performance. Briefly, the number of MM used in the assay is optimized to have enough binding sites for the formation of complexes with the highest clinically relevant concentration of the analyte in the samples (to reach the highest c-$Ab_{Aβ-42}$ concentration). Even a higher amount of MM produced a higher signal, they gave rise to aggregations, diminishing the active surface and lowering the effective navigation to capture the

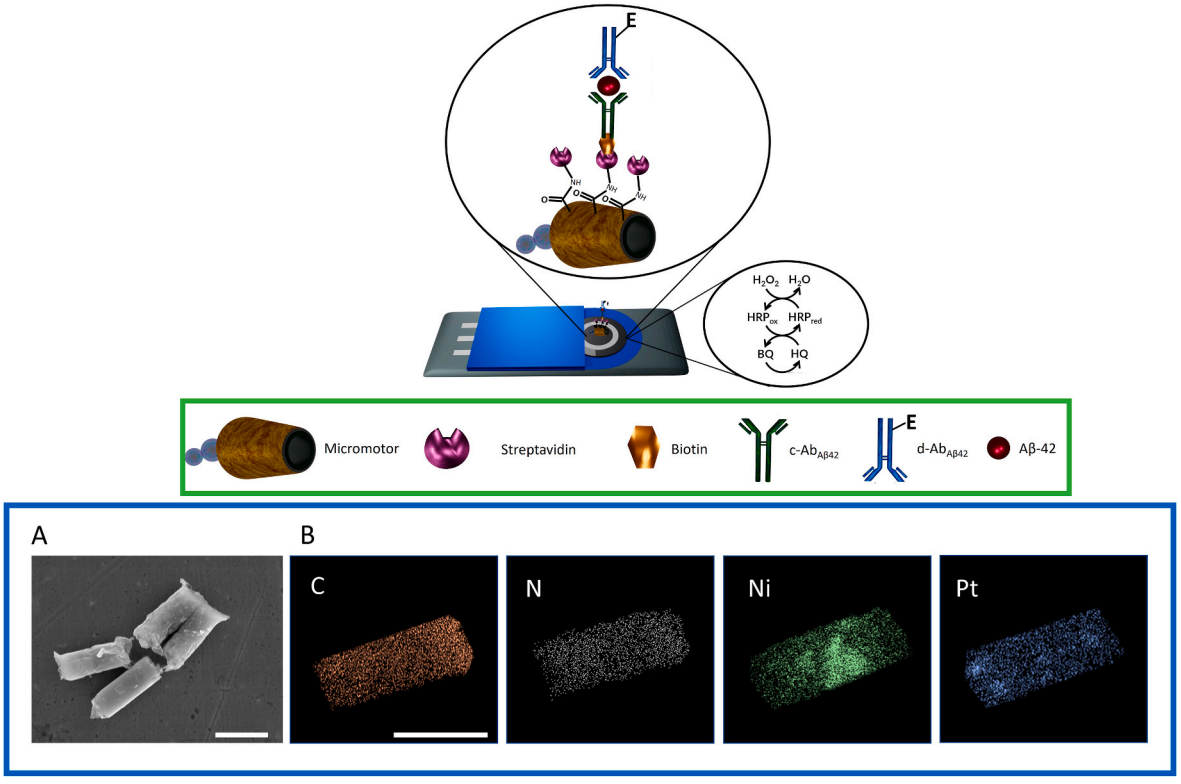

Fig. 1. Sandwich-type MM-based electrochemical immunoassay for Aβ-42. (Top), SEM images (A), and EDX analysis (B) of PPy/Ni/PtNPs micromotors (bottom). Scale bar: 10 μm SEM images and 9 μm EDX images.

analyte molecules. The high signal in controls can be due to the non-specific binding of HRP-labelled detection antibody (d-$Ab_{Aβ-42}$) onto the MM surface especially in higher amounts of them. For this reason, the optimized amount of micromotors was chosen to have enough binding sites to form the highest amount of the immunocomplexes without such aggregation occurring. From the inspection of these studies, 5000 micromotors become as the optimum number due to the standard/sample (presence of Aβ-42) signal-to-blank (without Aβ-42) ratio. Streptavidin previously attached to the MM surface allowed the oriented immobilization of the specific antibody to be evaluated in the range between 200 and 800 μg/mL. The optimal amount of 400 μg/mL ensures the modification of the active surface of MM.

After optimization of the number of MM and their functionalization with streptavidin, the concentration of c-$Ab_{Aβ-42}$ on the surface of MM was studied in a range of 5–50 μg/mL. At set MM number, this variable showed an important influence as shown in Fig. S1B. The highest signal was obtained at 25 μg/mL, while higher values displayed a lower signal, probably due to steric hindrance produced by the excess of c-$Ab_{Aβ-42}$ on the MM surface. In addition, the time needed for antibody immobilization was evaluated in the 15–60 min range. 30 min. reached the highest signal, while higher times could produce excess agglomeration of MM or immobilized cAb molecules, reducing the MM-based immunoassay efficiency (Fig. S1C). BSA used to reduce nonspecific binding of the analyte or detection antibody onto the MM surface was also tested in a range of 1–10 % (w/v). 5% BSA was directly added to the sample solution to prevent non-specific binding.

Once the functionalized MM was adequately optimized, those variables related to the on-the-fly immunoassay were also studied. This includes the concentration of d-$Ab_{Aβ-42}$, the sample volume, and the recognition time as well as propulsion conditions.

d-$Ab_{Aβ-42}$ was tested in a range of 0.25–1.5 μg/mL, even in the presence and absence of the Aβ-42 through the autonomous propulsion of micromotors. The highest signal was obtained with 1 μg/mL d-$Ab_{Aβ-42}$ ensuring the efficient labeling of all Aβ-42 captured onto the c-$Ab_{Aβ-42}$-MM (Fig. S2A). Looking at Fig. S2B, sample volume had a notable influence on the analytical signal. As can be observed, 25 μL of sample is needed to obtain better results. A higher volume sample probably reduces the chance of finding the existing analyte molecules at any given time for the used optimized amount of MM. Recognition time during the on-the-fly step was also studied between 5 and 60 min. In this sense, 15 min produced the best result since higher times cause agglomeration of MM, excess bubble formation that prevents the correct movement of MM, reducing the formation of the immunocomplexes, and inactivation of peroxidase enzyme due to the presence of high H_2O_2 concentration needed for propulsion (Fig. S2C). A comparison of the effectiveness of the self-propelled motion of MM versus static or stirring conditions is provided in Fig. S3. The on-the-fly recognition produces an improved performance in comparison with the controls (static and conventional stirring conditions), being 2% v/v H_2O_2 as the adequate fuel concentration. Higher fuel concentrations cause the same negative effects previously commented on for recognition time discussion. Briefly, the variables tested and selected values are listed in Table 1.

Table 1
Optimization of PPy/Ni/PtNPs MM-based immunoassay for Aβ-42 detection.

Assay step	Parameter	Tested Range	Selected Value
Formation Immunocomplex	**Micromotors quantity, number**	2400–10000	5000
	[Streptavidin] , μg/mL	200–800	400
	[c-$Ab_{Aβ42}$] , μg/mL	5–50	25
	c-$Ab_{Aβ42}$ time, min.	15–60	30
On-the-fly recognition	**[d-$Ab_{Aβ42}$] , μg/mL**	0.25-1.5	1
	Block step, [BSA] %	1–10	5
	Sample Volume, μL	2–50	25
	Recognition time, min.	5–60	15
	Fuel (H_2O_2), %	0–4	2

3.2. Analytical performance

The analytical performance of the MM-based immunoassay was carefully studied (see Table S1 for analytical figures of merit). The sigmoidal and the linear calibration plots obtained were shown in Fig. 2A, with a working linear range between 0.2 and 50 ng/mL ($r = 0.997$, $EC_{50} = 1.9$ ng/mL) covering the clinically relevant concentrations with high sensitivity, LOD: 0.06 ng/mL and LOQ: 0.2 ng/mL. Precision was also studied at three concentration levels (0.2, 2, and 50 ng/mL) with values (in amperometric signals) of $RSD_{0.2} = 5.8\%$, $RSD_2 = 7.5\%$, and $RSD_{50} = 4.8\%$ for intra-assay studies ($n = 5$). On the other hand, the stability of the c-$Ab_{Aβ-42}$-MM conjugates was tested under storage at 4 °C in 25 μL of PBS. They were prepared on the same day, stored, and used to construct immunoassay on different days and measure 2 ng/mL Aβ-42 solutions. The amperometric responses remained during at least 50 days within the control limits set by ±3 times the standard deviation of the measurements ($n = 5$) carried out on the first day, decreasing the amperometric signal by 2% from day 55. (Fig. 2B). This excellent storage stability suggests the possibility of preparing a set of c-$Ab_{Aβ-42}$-MM conjugates and storing them under the above-mentioned conditions until their use for the preparation of the immunosensors was requested, subsequently lowering the overall immunoassay analysis times.

3.3. Analysis of diagnosed Alzheimer's BT, CSF, and plasma samples

The analytical potential of MM technology was explored in the analysis of Aβ-42 in three clinical sample classes with high significance and with different analytical challenges in terms of selectivity, sensitivity, sample availability, and diagnosis purpose. Table 2 summarizes the main clinical features of the AD samples and their analytical determination challenges: left prefrontal cortex BT (high selectivity is required due to the plethora of compounds potentially present; *post-mortem*, no alive biopsy sample can be obtained, non-invasive *-post mortem-*), CSF (both selectivity and sensitivity are challenged, being sensitivity the most relevant since cleaner sample is expected, invasive), and the plasma (high selectivity is required regarding the number of proteins and the highly abundance of the fifteen most abundant proteins, high sensitivity is also needed due to biomarkers dilution in blood, minimally invasive, the final sample target to avoid any biopsy and to help in alive early diagnosis as well).

Table 3 lists the Aβ-42 levels obtained using the MM-based immunoassay and the reference values obtained with the single molecule counting technology (SMCx). The high agreement between the micromotors-based Aβ-42 levels with the clinical values obtained with the SMCx technology for all the BT, CFL, and plasma samples analyzed showed the potential of the MM approach for the analysis of the golden AD biomarker Aβ-42. Also, both sets of data exhibited an excellent correlation performance ($r > 0.9990$, $p < 0.05$). Although there is no established consensus on the indicative levels of this biomarker in samples that ensure the existence of the AD disease, our approach (LOQ = 0.2 ng/mL) allows the reliable determination of Aβ-42 in BT, CSF, and plasma. The levels found in BT, CSF, and plasma samples from AD patients were coincident using both methodologies (MM-based immunoassay and SMCx), which indicates the adequate analytical behavior of the MM-based immunoassay to perform early or confirmatory diagnoses and longitudinal studies (particularly relevant in diseases with long clinical phases such as AD).

It is also important to highlight that good results have been obtained by analyzing three very different types of matrices. An example can be visualized with the data obtained for **patient 1** whose results show a high agreement with the results obtained with SMCx in two different matrices (plasma and BT), confirming the high versatility of our approach to measure different biological/clinical samples without

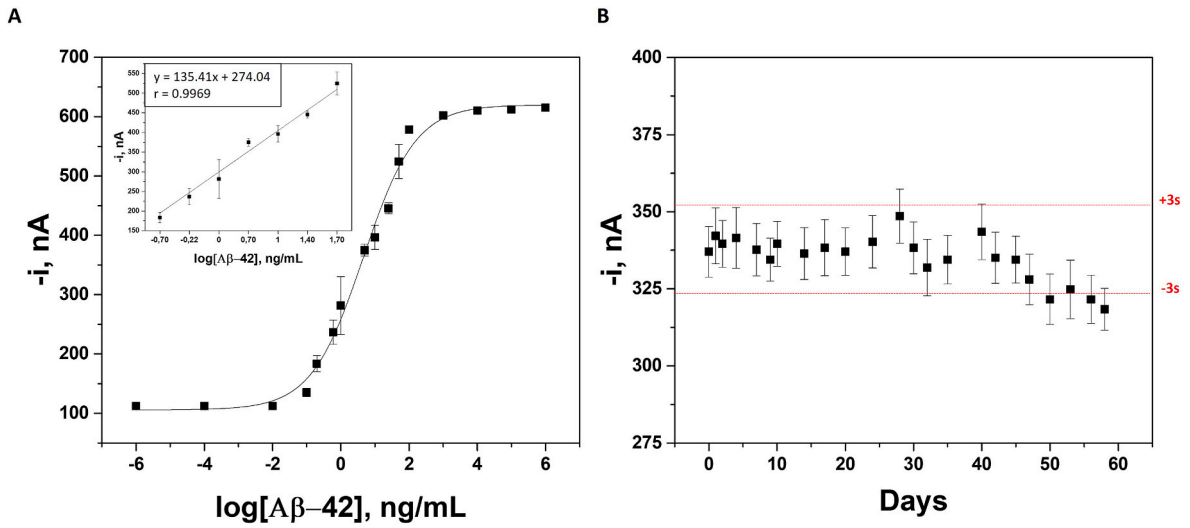

Fig. 2. Analytical performance for amperometric determination of Aβ-42 using an MM-assisted immunoassay. (A) Sigmoidal curve and the calibration plots; (B) Amperometric response from the immunoassay from the stored anti-Aβ-42 (c-Ab = 25 μg/mL, Aβ-42 = 2 ng/mL) functionalized MM. Control limits (red lines) were calculated as 3 × mean values of three amperometric responses obtained on the preparation day. Conditions are described in Table 1.

Table 2
Main features, challenges, and types of diagnosis of Alzheimer's disease allowed by the three types of samples analyzed.

Sample	Clinical key features	Selectivity	Sensitivity	Invasive	Biodisponibility	Diagnosis
BT	AD (Braak IV, V, and VI) and healthy	+++	++	Post mortem	Post mortem	Not applicable
CSF	AD (Braak III, IV, V, and VI) and healthy	+	+++	+++	Alive	Early
Plasma	AD (Braak IV, V, and IV) and healthy	+++	++	+	Alive	Early

+, ++, and +++ denote low, medium, and highly challenging respectively.

Table 3
Analysis of BT, CFL, and plasma samples from control subjects and Alzheimer patients.

Samples	MM (pg/mL)	SMCx (pg/mL)	Er (%)
Tissue			
Control 1 Female, age: 61 years, Healthy	293 ± 41	293	0.3
Control 2 Male, age: 74 years, Healthy	89 ± 11	<80	11
Patient 1 Female, age: 91 years, AD Braak IV	735 ± 170	688	7
Patient 2 Female, age: 88 years, AD Braak VI	2289 ± 634	2166	6
Cerebrospinal fluid			
Control 3 Female, age: 84 years, Healthy	171 ± 20	164	1
Patient 3 Male, age: 85 years, AD Braak IV	212 ± 26	184	15
Patient 4 Male, age: 87 years, AD Braak V	684 ± 41	650	5
Patient 5 Male, age: 91 years, AD Braak VI	1026 ± 60	972	4
Plasma			
Control 2 Male, age: 74 years, Healthy	209	196	4
Patient 1 Female, age: 91 years, AD Braak IV	289	300	4
Patient 6 Female, age: 86 years, AD Braak V	277	289	4

losing the efficiency of the process (Fig. S4). This feasibility would allow the diagnosis of the disease with plasma, the less invasive sample, and CSF. Despite using a low number of samples, ROC curve analyses performed either with the data from the MM or with the SMCx displayed similar results with complete discrimination between AD samples and controls (Fig. S4).

Related to the comparison of our reported work with others described in the literature for the determination of Aβ-42, it is important to remark that since the MM approach is pioneering a direct comparison with other technologies is not fully pertinent. However, our approach combined shorter analysis times (15 min) (Li et al., 2019; Liu et al., 2014; Zhang et al., 2019), with better sensitivities (Deng et al., 2018; Li et al., 2019), and even the use of lower sample volumes (Veloso et al., 2014). Indeed, the fact that the MM performs the Aβ-42 detection on-the-fly, and the washing stages carried out, minimize the matrix effect, and allows the direct determination of the undiluted samples by simple interpolation in the calibration plot, covering the clinically relevant concentrations in all samples studied. It simplifies the user's analytical operation and together with the affordability and use of disposable electrodes and amperometry transduction is an added value for future POCT.

It is also important to highlight that commercially available ELISA kits, commonly adopted in this field (e.g. https://www.rndsystems.com/products/human-amyloid-beta-aa1-42-quantikine-elisa.kit_dab142#product-datasheets) and validated for the determination of cell culture supernatants, tissue lysates, and CSF but not for plasma samples, more challenging for the low concentration due to the blood-brain barrier, required 4.5 h unlike the 15 min of the proposed technology (starting from the c-Ab pre-coated plate or c-Ab-MM, respectively). Indeed, the unique features offered by the enhanced MM-assisted immunosensing coupled with electrochemical transduction in terms of cost and portability made the proposed technology ideal for translational progress beyond the well-controlled laboratory bench toward the portable in-field devices for outpatient and hospital routine or even for low-resource settings.

Additionally, in our approach, a set of unique real samples of AD patients were analyzed, which allowed us to glimpse the high potential of MM technology in the field of biosensors, which, although in an adolescent stage, is also offered as a competitive alternative to other

biosensors and clinically established approaches.

4. Conclusions

The first MM-based immunoassay for fast and accurate determination of Aβ-42 in Alzheimer's diagnosed clinical samples with high significance has successfully been developed. The immunoassay through an on-the-fly recognition of Aβ-42 was performed speedily (15 min), with a high sensitivity (0.06 ng/mL), and in a low volume of clinical BT, CSF or plasma samples (25 μL) with a linear range that covered the clinical levels, allowing the direct determination without any dilution, reducing the complexity of the analysis. Our approach exhibited an excellent agreement with the declared diagnosed values in BT, CSF, and plasma samples from clinical AD patients obtained with SMCx. Remarkably, although the detection of a single biomarker is not enough for AD diagnosis, the results presented here highlight the potential of MM for diagnosis using a plethora of samples with small volumes. Even more importantly, this approach opens new noninvasive capabilities for AD diagnosis through the possibility of reaching a multiplex detection in plasma samples of several biomarkers to improve the blood-based diagnosis of Alzheimer's disease.

However, the transfer of this technology to the clinic and its acceptance and incorporation into clinical practice will be difficult and time-consuming tasks. Overcoming the complex challenges involved requires close collaborations with hospitals and commercial/public entities interested in transferring the technology. The adoption of these new devices in a clinical environment requires not only that laboratory personnel become familiar with the new methodologies, but also that the medical personnel expand their knowledge about this technology and how to implement it in their clinical routine. Widespread use of new AD biomarker tools in the clinic also requires comprehensive standardization and validation approaches, which must be addressed with sufficient consistency to withstand the onslaught that the clinical diagnostics industry will launch.

CRediT authorship contribution statement

José M. Gordón Pidal: Writing – review & editing, Writing – original draft, Visualization, Methodology, Investigation, Formal analysis, Data curation, Conceptualization. **María Moreno-Guzmán:** Writing – review & editing, Visualization, Supervision, Methodology, Investigation, Formal analysis, Data curation, Conceptualization. **Ana Montero-Calle:** Writing – review & editing, Investigation, Formal analysis, Data curation. **Alejandro Valverde:** Writing – review & editing, Visualization, Methodology, Investigation. **José M. Pingarrón:** Writing – review & editing, Supervision. **Susana Campuzano:** Writing – review & editing, Supervision, Funding acquisition. **Miguel Calero:** Writing – review & editing, Formal analysis, Data curation. **Rodrigo Barderas:** Writing – review & editing, Resources, Formal analysis, Data curation. **Miguel Ángel López:** Writing – review & editing, Supervision, Formal analysis, Conceptualization. **Alberto Escarpa:** Writing – review & editing, Supervision, Resources, Project administration, Funding acquisition, Formal analysis, Conceptualization.

Declaration of competing interest

The authors declare that they have no known competing financial interests or personal relationships that could have appeared to influence the work reported in this paper.

Data availability

No data was used for the research described in the article.

Acknowledgments

This research was supported by Grants PID2020-118154GB-I00 funded by MCIN/AEI/ 10.13039/501100011033 (M.M.G., M.A.L., and A. E) and PID2019-110401RB-100 (M.C.) and supported by the TRANSNANOAVANSES program (S2018/NMT-4349 (A.E., M-A.L., M. M.G., J.M.G-P., A.V., S.C.)) and Y2020/NMT6312 (NEURO-CHIP-CM) program (A.E.) from the Community of Madrid. M.A.L. and A.E. also acknowledge funding from the DISCOVER-UAH-CM Project (Ref. REACT UE-CM2021-01), co-founded by the Community of Madrid (CAM) and European Union (UE), through the European Regional Development Fund (ERDF) and supported as part of the EU's response to COVID-19 pandemic. A. V. acknowledges a predoctoral contract from Complutense University of Madrid. A. M-C. acknowledges a FPU predoctoral contract from the Spanish Ministerio de Educación, Cultura y Deporte.

Appendix A. Supplementary data

Supplementary data to this article can be found online at https://doi.org/10.1016/j.bios.2023.115988.

References

Ah, J., Kim, M., Min, S., Taek, K., Song, T., 2015. Magnetic bead droplet immunoassay of oligomer amyloid β for the diagnosis of Alzheimer ′ s disease using micro-pillars to enhance the stability of the oil – water interface. Biosens. Bioelectron. 67, 724–732. https://doi.org/10.1016/j.bios.2014.10.042.

Alzheimer's disease facts and figures, 2021. Alzheimer's Dement. 17, 327–406. https://doi.org/10.1002/alz.12328.

Baumgart, M., Snyder, H.M., Carrillo, M.C., Fazio, S., Kim, H., Johns, H., 2015. Summary of the evidence on modifiable risk factors for cognitive decline and dementia: a population-based perspective. Alzheimer's Dement. 11, 718–726. https://doi.org/10.1016/j.jalz.2015.05.016.

Brown, R.C., Lockwood, A.H., Sonawane, B.R., 2005. Neurodegenerative diseases: an Overview of environmental risk factors. Environ. Health Perspect. 113, 1250–1256. https://doi.org/10.1289/ehp.7567.

Calabrò, M., Rinaldi, C., Santoro, G., Crisafulli, C., 2021. The biological pathways of Alzheimer disease: a review. AIMS Neurosci 8, 86–132. https://doi.org/10.3934/Neuroscience.2021005.

Deng, C., Liu, H., Zhang, M., Deng, H., Lei, C., Shen, L., Jiao, B., Tu, Q., Jin, Y., Xiang, L., Deng, W., Xie, Y., Xiang, J., 2018. A Light-up non-thiolated aptasensor for low-mass soluble amyloid- 40 oligomers at high salt concentrations. Anal. Chem. 90, 1710–1717. https://doi.org/10.1021/acs.analchem.7b03468.

Deture, M.A., Dickson, D.W., 2019. The neuropathological diagnosis of Alzheimer's disease. Mol. Neurodegener. 14, 32. https://doi.org/10.1186/s13024-019-0333-5.

Feng, Y., Chang, X., Liu, H., Hu, Y., Li, T., Li, L., 2021. Multi-response biocompatible Janus micromotor for ultrasonic imaging contrast enhancement. Appl. Mater. Today 23, 101026. https://doi.org/10.1016/j.apmt.2021.101026.

Franzmeier, N., Rubinski, A., Neitzel, J., Kim, Y., Damm, A., Na, D.L., Kim, H.J., Lyoo, C. H., Cho, H., Finsterwalder, S., Duering, M., Seo, S.W., Ewers, M., 2019. Functional connectivity associated with tau levels in ageing, Alzheimer's, and small vessel disease. Brain 142, 1093–1107. https://doi.org/10.1093/brain/awz026.

Gao, W., Sattayasamitsathit, S., Uygun, A., Pei, A., Ponedal, A., Wang, J., 2012. Polymer-based tubular microbots: Role of composition and preparation. Nanoscale 4, 2447–2453. https://doi.org/10.1039/c2nr30138e.

Garranzo-Asensio, M., Segundo-Acosta, P.S., Martínez-Useros, J., Montero-Calle, A., Fernández-Aceñero, M.J., Häggmark-Månberg, A., Pelaez-Garcia, A., Villalba, M., Rabano, A., Nilsson, P., Barderas, R., 2018. Identification of prefrontal cortex protein alterations in Alzheimer's Disease. Oncotarget 9, 10847–10867. https://doi.org/10.18632/oncotarget.24303.

Gordón, J., Arruza, L., Ibáñez, M.D., Moreno-Guzmán, M., López, M.A., Escarpa, A., 2022. On the move-sensitive fluorescent aptassay on board catalytic micromotors for the determination of Interleukin-6 in Ultra-low serum volumes for neonatal sepsis diagnostics. ACS Sens. 7, 3144–3152. https://doi.org/10.1021/acssensors.2c01635.

Gordón Pidal, J.M., Arruza, L., Moreno-Guzmán, M., López, M.A., Escarpa, A., 2023. OFF-ON on-the-fly aptassay for rapid and accurate determination of procalcitonin in very low birth weight infants with sepsis suspicion. Sensors Actuators B Chem 378, 133107. https://doi.org/10.1016/j.snb.2022.133107.

Haes, A.J., Chang, L., Klein, W.L., Van Duyne, R.P., 2005. Detection of a biomarker for Alzheimer's disease from synthetic and clinical samples using a nanoscale optical biosensor. J. Am. Chem. Soc. 127, 2264–2271. https://doi.org/10.1021/ja044087q.

Hampel, H., Hardy, J., Blennow, K., Chen, C., Perry, G., Kim, S.H., Villemagne, V.L., Aisen, P., Vendruscolo, M., Iwatsubo, T., Masters, C.L., Cho, M., Lannfelt, L., Cummings, J.L., Vergallo, A., 2021. The amyloid-β Pathway in alzheimer's disease. Mol. Psychiatry 26, 5481–5503. https://doi.org/10.1038/s41380-021-01249-0.

Hampel, H., Vergallo, A., Caraci, F., Cuello, A.C., Lemercier, P., Vellas, B., Giudici, K.V., Baldacci, F., Hänisch, B., Haberkamp, M., Broich, K., Nisticò, R., Emanuele, E., Llavero, F., Zugaza, J.L., Lucía, A., Giacobini, E., Lista, S., 2020. Future avenues for

Alzheimer's disease detection and therapy: liquid biopsy, intracellular signaling modulation, systems pharmacology drug discovery. Neuropharmacology 185, 108081. https://doi.org/10.1016/j.neuropharm.2020.108081.
Jack, C.R., Knopman, D.S., Jagust, W.J., Shaw, L.M., Aisen, P.S., Weiner, M.W., Petersen, R.C., Trojanowski, J.Q., 2010. Hypothetical model of dynamic biomarkers of the Alzheimer's pathological cascade. Lancet Neurol. 9, 119–128. https://doi.org/10.1016/S1474-4422(09)70299-6.
Klaver, A.C., Patrias, L.M., Coffey, M.P., Finke, J.M., Loeffler, D.A., 2010. Measurement of anti-Aβ1-42 antibodies in intravenous immunoglobulin with indirect ELISA: the problem of nonspecific binding. J. Neurosci. Methods 187, 263–269. https://doi.org/10.1016/j.jneumeth.2010.01.018.
Kühbach, K., Hülsemann, M., Herrmann, Y., Kravchenko, K., Kulawik, A., Linnartz, C., Peters, L., Wang, K., Willbold, J., Willbold, D., Bannach, O., 2016. Application of an amyloid beta oligomer standard in the sFIDA. Assay. Front. Neurosci. 10, 8. https://doi.org/10.3389/fnins.2016.00008.
Kulawik, A., Heise, H., Zafiu, C., Willbold, D., Bannach, O., 2018. Advancements of the sFIDA method for oligomer-based diagnostics of neurodegenerative diseases. FEBS Lett. 592, 516–534. https://doi.org/10.1002/1873-3468.12983.
Lane, C.A., Hardy, J., Schott, J.M., 2018. Alzheimer's disease. Eur. J. Neurol. 25, 59–70. https://doi.org/10.1111/ene.13439.
Li, C., Yang, L., Han, Y., Wang, X., 2019. A simple approach to quantitative determination of soluble amyloid-β peptides using a ratiometric fluorescence probe. Biosens. Bioelectron. 142, 111518 https://doi.org/10.1016/j.bios.2019.111518.
Liu, B., Shen, H., Hao, Y., Zhu, X., Li, S., Huang, Y., Qu, P., Xu, M., 2018. Lanthanide functionalized Metal-Organic Coordination polymer: toward novel Turn-on fluorescent sensing of amyloid β-peptide. Anal. Chem. 90, 12449–12455. https://doi.org/10.1021/acs.analchem.8b01546.
Liu, L., He, Q., Zhao, F., Xia, N., Liu, H., Li, S., Liu, R., Zhang, H., 2014. Competitive electrochemical immunoassay for detection of β-amyloid (1-42) and total β-amyloid peptides using p-aminophenol redox cycling. Biosens. Bioelectron. 51, 208–212. https://doi.org/10.1016/j.bios.2013.07.047.
Lukiw, W.J., Vergallo, A., Lista, S., Hampel, H., Zhao, Y., 2020. Biomarkers for alzheimer's disease (Ad) and the application of precision medicine. J. Pers. Med. 10, 138. https://doi.org/10.3390/jpm10030138.
Lv, G., Sun, A., Wei, P., Zhang, N., Lan, H., Yi, T., 2016. A spiropyran-based fluorescent probe for the specific detection of β-amyloid peptide oligomers in Alzheimer's disease. Chem. Commun. 52, 8865–8868. https://doi.org/10.1039/c6cc02741e.
Maria-Hormigos, R., Jurado-Sánchez, B., Escarpa, A., 2016a. Labs-on-a-chip meet self-propelled micromotors. Lab Chip 16, 2397–2407. https://doi.org/10.1039/c6lc00467a.
Maria-Hormigos, R., Jurado-Sanchez, B., Vazquez, L., Escarpa, A., 2016b. Carbon Allotrope nanomaterials based catalytic micromotors. Chem. Mater. 28, 8962–8970. https://doi.org/10.1021/acs.chemmater.6b03689.
María-Hormigos, R., Molinero-Fernández, Á., López, M.Á., Jurado-Sánchez, B., Escarpa, A., 2022. Prussian Blue/Chitosan micromotors with Intrinsic enzyme-like Activity for (bio)-Sensing assays. Anal. Chem. 94, 5575–5582. https://doi.org/10.1021/acs.analchem.1c05173.
Masters, C.L., Bateman, R., Blennow, K., Rowe, C.C., Sperling, R.A., Cummings, J.L., 2015. Alzheimer's disease. Nat. Rev. Dis. Prim. 1, 15056 https://doi.org/10.1038/nrdp.2015.56.
Molinero-Fernandez, A., Lopez, M.A., Escarpa, A., 2020. Electrochemical Microfluidic micromotors-based immunoassay for C-reactive protein determination in Preterm neonatal samples with sepsis suspicion. Anal. Chem. 92, 5048–5054. https://doi.org/10.1021/acs.analchem.9b05384.
Molinero-Fernández, Á., Moreno-Guzmán, M., Arruza, L., López, M.Á., Escarpa, A., 2020. Polymer-based micromotor fluorescence immunoassay for on-the-move sensitive procalcitonin determination in very low birth weight infants' plasma. ACS Sens. 5, 1336–1344. https://doi.org/10.1021/acssensors.9b02515.
Montero-Calle, A., Coronel, R., Garranzo-Asensio, M., Solís-Fernández, G., Rábano, A., de los Ríos, V., Fernández-Aceñero, M.J., Mendes, M.L., Martínez-Useros, J., Megías, D., Moreno-Casbas, M.T., Peláez-García, A., Liste, I., Barderas, R., 2023a. Proteomics analysis of prefrontal cortex of Alzheimer's disease patients revealed dysregulated proteins in the disease and novel proteins associated with amyloid-β pathology. Cell. Mol. Life Sci. 80, 141. https://doi.org/10.1007/s00018-023-04791-y.
Montero-Calle, A., Garranzo-Asensio, M., Torrente-Rodríguez, R.M., Ruiz-Valdepeñas Montiel, V., Poves, C., Dziaková, J., Sanz, R., Díaz Del Arco, C., Pingarrón, J.M., Fernández-Aceñero, M.J., Campuzano, S., Barderas, R., 2023b. p53 and p63 Proteoforms Derived from alternative Splicing possess Differential Seroreactivity in Colorectal Cancer with Distinct diagnostic ability from the Canonical proteins. Cancers 15 (7), 2102. https://doi.org/10.3390/cancers15072102.
Montero-Calle, A., San Segundo-Acosta, P., Garranzo-Asensio, M., Rábano, A., Barderas, R., 2020. The molecular Misreading of APP and UBB Induces a Humoral Immune response in alzheimer's disease patients with diagnostic ability. Mol. Neurobiol. 57, 1009–1020. https://doi.org/10.1007/s12035-019-01809-0.
Mundaca-Uribe, R., Karshalev, E., Esteban-Fernández de Ávila, B., Wei, X., Nguyen, B., Litvan, I., Fang, R.H., Zhang, L., Wang, J., 2021. A Microstirring Pill Enhances Bioavailability of Orally Administered Drugs. Adv. Sci. 8, 2100389 https://doi.org/10.1002/advs.202100389.
Murphy, M.P., Levine, H., 2010. Alzheimer's disease and the amyloid-β peptide. J. Alzheimers. Dis. 19, 311–323. https://doi.org/10.3233/JAD-2010-1221.
Nguyen, T.T., Nguyen, T.D., Nguyen, T.K.O., Vo, T.K., Vo, V.G., 2021. Advances in developing therapeutic strategies for Alzheimer's disease. Biomed. Pharmacother. 139, 111623 https://doi.org/10.1016/j.biopha.2021.111623.
Niccoli, T., Partridge, L., 2012. Ageing as a risk factor for disease. Curr. Biol. 22, R741–R752. https://doi.org/10.1016/j.cub.2012.07.024.
Novotný, F., Plutnar, J., Pumera, M., 2019. Plasmonic self-propelled nanomotors for Explosives detection via solution-based surface enhanced Raman Scattering. Adv. Funct. Mater. 29, 1903041 https://doi.org/10.1002/adfm.201903041.
Ono, M., Watanabe, H., Kitada, A., Matsumura, K., Ihara, M., Saji, H., 2016. Highly selective tau-SPECT imaging probes for detection of neurofibrillary tangles in Alzheimer's disease. Sci. Rep. 6, 34197 https://doi.org/10.1038/srep34197.
Pacheco, M., López, M.Á., Jurado-Sánchez, B., Escarpa, A., 2019. Self-propelled micromachines for analytical sensing: a critical review. Anal. Bioanal. Chem. 411, 6561–6573. https://doi.org/10.1007/s00216-019-02070-z.
Palareti, G., Legnani, C., Cosmi, B., Antonucci, E., Erba, N., Poli, D., Testa, S., Tosetto, A., 2016. Comparison between different D-Dimer cutoff values to assess the individual risk of recurrent venous thromboembolism: analysis of results obtained in the DULCIS study. Int. J. Lab. Hematol. 38, 42–49. https://doi.org/10.1111/ijlh.12426.
Perry, D.C., Sturm, V.E., Peterson, M.J., Pieper, C.F., Bullock, T., Boeve, B.F., Miller, B.L., Guskiewicz, K.M., Berger, M.S., Kramer, J.H., Welsh-Bohmer, K.A., 2016. Association of traumatic brain injury with subsequent neurological and psychiatric disease: a meta-analysis. J. Neurosurg. 124, 511–526. https://doi.org/10.3171/2015.2.JNS14503.
Qin, J., Su, J., Gyu, D., Cho, M., Lee, Y., 2018. Curcumin-based electrochemical sensor of amyloid- β oligomer for the early detection of Alzheimer ' s disease. Sensors Actuators B. Chem. 273, 1593–1599. https://doi.org/10.1016/j.snb.2018.07.078.
San Segundo-Acosta, P., Montero-Calle, A., Fuentes, M., Rábano, A., Villalba, M., Barderas, R., 2019. Identification of alzheimer's disease Autoantibodies and their target biomarkers by phage Microarrays. J. Proteome Res. 18, 2940–2953. https://doi.org/10.1021/acs.jproteome.9b00258.
San Segundo-Acosta, P., Montero-Calle, A., Jernbom-Falk, A., Alonso-Navarro, M., Pin, E., Andersson, E., Hellström, C., Sánchez-Martínez, M., Rábano, A., Solís-Fernández, G., Peláez-García, A., Martínez-Useros, J., Fernández-Aceñero, M.J., Månberg, A., Nilsson, P., Barderas, R., 2021. Multiomics Profiling of alzheimer's disease serum for the identification of Autoantibody biomarkers. J. Proteome Res. 20, 5115–5130. https://doi.org/10.1021/acs.jproteome.1c00630.
Se Thoe, E., Fauzi, A., Tang, Y.Q., Chamyuang, S., Chia, A.Y.Y., 2021. A review on advances of treatment modalities for Alzheimer's disease. Life Sci. 276, 119129 https://doi.org/10.1016/j.lfs.2021.119129.
Selkoe, D.J., 2001. Alzheimer's disease: genes, proteins, and therapy. Physiol. Rev. 81, 741–766. https://doi.org/10.1152/physrev.2001.81.2.741.
Selkoe, D.J., Schenk, D., 2003. Alzheimer's disease: Molecular Understanding Predicts amyloid-based therapeutics. Annu. Rev. Pharmacol. Toxicol. 43, 545–584. https://doi.org/10.1146/annurev.pharmtox.43.100901.140248.
Shankar, G.M., Li, S., Mehta, T.H., Garcia-Munoz, A., Shepardson, N.E., Smith, I., Brett, F. M., Farrell, M.A., Rowan, M.J., Lemere, C.A., Regan, C.M., Walsh, D.M., Sabatini, B. L., Selkoe, D.J., 2008. Amyloid-β protein dimers isolated directly from Alzheimer's brains impair synaptic plasticity and memory. Nat. Med. 14, 837–842. https://doi.org/10.1038/nm1782.
Taylor, J.P., Hardy, J., Fischbeck, K.H., 2002. Toxic proteins in neurodegenerative disease. Science 296, 1991–1995. https://doi.org/10.1126/science.1067122.
Teoh, C.L., Su, D., Sahu, S., Yun, S.W., Drummond, E., Prelli, F., Lim, S., Cho, S., Ham, S., Wisniewski, T., Chang, Y.T., 2015. Chemical fluorescent probe for detection of Aβ oligomers. J. Am. Chem. Soc. 137, 13503–13509. https://doi.org/10.1021/jacs.5b06190.
Thorsell, A., Bjerke, M., Gobom, J., Brunhage, E., Vanmechelen, E., Andreasen, N., Hansson, O., Minthon, L., Zetterberg, H., Blennow, K., 2010. Neurogranin in cerebrospinal fluid as a marker of synaptic degeneration in Alzheimer's disease. Brain Res. 1362, 13–22. https://doi.org/10.1016/j.brainres.2010.09.073.
Torrente-Rodríguez, R.M., Montero-Calle, A., San Bartolomé, C., Cano, O., Vázquez, M., Iglesias-Caballero, M., Corral-Lugo, A., McConnell, M.J., Pascal, M., Mas, V., Pingarrón, J.M., Barderas, R., Campuzano, S., 2022. Towards control and Oversight of SARS-CoV-2 diagnosis and monitoring through multiplexed quantitative Electroanalytical Immune response biosensors. Angew. Chem. Int. Ed. 61, e202203662 https://doi.org/10.1002/anie.202203662.
Veloso, A.J., Chow, A.M., Ganesh, H.V.S., Li, N., Dhar, D., Wu, D.C.H., Mikhaylichenko, S., Brown, I.R., Kerman, K., 2014. Electrochemical immunosensors for effective evaluation of amyloid-beta modulators on oligomeric and fibrillar aggregation processes. Anal. Chem. 86, 4901–4909. https://doi.org/10.1021/ac500424t.
Wang, J., 2014. Nanomachines. Fundamentals and applications. Angew. Chem. Int. Ed. 53, 4274–4275. https://doi.org/10.1002/anie.201311274.
Wang, J., 2016. Self-propelled affinity biosensors: Moving the receptor around the sample. Biosens. Bioelectron. 76, 234–242. https://doi.org/10.1016/j.bios.2015.04.095.
Wesenhagen, K.E.J., Teunissen, C.E., Visser, P.J., Tijms, B.M., 2020. Cerebrospinal fluid proteomics and biological heterogeneity in Alzheimer's disease: a literature review. Crit. Rev. Clin. Lab Sci. 57, 86–98. https://doi.org/10.1080/10408363.2019.1670613.
Xia, N., Zhou, B., Huang, N., Jiang, M., Zhang, J., Liu, L., 2016. Visual and fluorescent assays for selective detection of beta-amyloid oligomers based on the inner filter effect of gold nanoparticles on the fluorescence of CdTe quantum dots. Biosens. Bioelectron. 85, 625–632. https://doi.org/10.1016/j.bios.2016.05.066.
Yi, X., Feng, C., Hu, S., Li, H., Wang, J., 2015. Surface plasmon resonance biosensors for simultaneous monitoring of amyloid-beta oligomers and fibrils and screening of select modulators. Analyst 141, 331–336. https://doi.org/10.1039/c5an01864a.
You, M., Yang, S., An, Y., Zhang, F., He, P., 2020. A novel electrochemical biosensor with molecularly imprinted polymers and aptamer-based sandwich assay for determining amyloid- β oligomer. J. Electroanal. Chem. 862, 114017 https://doi.org/10.1016/j.jelechem.2020.114017.

Yuan, K., Bujalance-Fernández, J., Jurado-Sánchez, B., Escarpa, A., 2020a. Light-driven nanomotors and micromotors: envisioning new analytical possibilities for biosensing. Microchim. Acta 187, 581. https://doi.org/10.1007/s00604-020-04541-y.

Yuan, K., Jiang, Z., Jurado-Sánchez, B., Escarpa, A., 2020b. Nano/micromotors for diagnosis and therapy of Cancer and Infectious diseases. Chem. Eur J. 26, 2309–2326. https://doi.org/10.1002/chem.201903475.

Yuan, K., Jurado-Sánchez, B., Escarpa, A., 2021. Dual-propelled Lanbiotic based Janus micromotors for selective inactivation of Bacterial Biofilms. Angew. Chem. Int. Ed. 60, 4915–4924. https://doi.org/10.1002/anie.202011617.

Zhang, Y., Figueroa-Miranda, G., Lyu, Z., Zafiu, C., Willbold, D., Offenhäusser, A., Mayer, D., 2019. Monitoring amyloid-B proteins aggregation based on label-free aptasensor. Sensors Actuators B Chem 288, 535–542. https://doi.org/10.1016/j.snb.2019.03.049.

Zhao, G., Pumera, M., 2013. Concentric bimetallic microjets by electrodeposition. RSC Adv. 3, 3963–3966. https://doi.org/10.1039/c3ra23128c.

Zhao, J., Chang, W., Liu, L., Xing, X., Zhang, C., Meng, H., Gopinath, S.C.B., Lakshmipriya, T., Chen, Y., Liu, Y., 2021. Graphene oxide-gold nanoparticle-aptamer complexed probe for detecting amyloid beta oligomer by ELISA-based immunoassay. J. Immunol. Methods 489, 112942. https://doi.org/10.1016/j.jim.2020.112942.

Zhou, Y., Lv, Y., Dong, H., Liu, L., Mao, G., Zhang, Y., 2021. Chemical Ultrasensitive assay of amyloid-beta oligomers using Au-vertical graphene/carbon cloth electrode based on poly (thymine) -templated copper nanoparticles as probes. Sensors Actuators B. Chem. 331, 129429 https://doi.org/10.1016/j.snb.2020.129429.

Zhu, X., Zhang, N., Zhang, Y., Liu, B., Chang, Z., Zhou, Y., Hao, Y., Ye, B., Xu, M., 2018. A sensitive gold nanoparticle-based aptasensor for colorimetric detection of Aβ1-40 oligomers. Anal. Methods 10, 641–645. https://doi.org/10.1039/c7ay02918g.